Noise in one-dimensional metamaterials supporting magnetoinductive lattice waves

R. R. A. Syms,* O. Sydoruk, and L. Solymar
Optical and Semiconductor Devices Group, Department of Electrical and Electronic Engineering, Imperial College London, Exhibition Road, London SW7 2AZ, United Kingdom
(Received 12 January 2013; revised manuscript received 10 April 2013; published 30 April 2013)

Equivalent circuit models are presented for the propagation of noise in one-dimensional negative-index metamaterials based on split-ring resonators (SRRs) and rods. The SRRs are modeled as lossy lumped-element *L*-*C* resonators, whose reactive components provide the effect of a negative relative permeability over a restricted frequency range but whose resistive elements act as sources of propagation loss and Johnson noise. Similarly, the rod loading is modeled as lumped-element inductors, whose reactive components provide the effect of a negative relative permittivity but whose resistive elements introduce further loss and noise. Coupling between the magnetic resonators allows the propagation of magnetoinductive lattice waves. The effect on the effective medium properties is to shift the apparent magnetic resonance up in frequency by an amount depending on the coupling coefficient and to allow the propagation of noise waves within the resonator array over the entire magnetoinductive band. The model predicts all the details of the electromagnetic and magnetoinductive noise inside the array. However, it is shown that the observable effect outside the array matches the prediction of a simplified model based only on the modified effective medium properties.

DOI: 10.1103/PhysRevB.87.155155 PACS number(s): 81.05.Xj, 41.20.Jb, 07.50.Hp

I. INTRODUCTION

Since the suggestion of Pendry[1] that electromagnetic (EM) media with negative effective parameters could be realized over a finite frequency range using split-ring resonators and rods, there has been considerable interest in metamaterials. Negative refraction was quickly demonstrated,[2,3] verifying a much earlier idea of Veselago.[4] Since then, attention has focused on the new applications made possible by media with controllable properties, such as near-field imaging and cloaking. However, for any application to be realistic, standard performance characteristics such as isotropy, spectral flatness, and loss must be considered. The last aspect is particularly important for metamaterials, which rely on lossy conductors to synthesize magnetic and dielectric properties. Even with high-conductivity metals, the *Q* factors that can be achieved in resonant structures at room temperature are low. Consequently propagation losses are high. While loss may be overcome using amplification, its inevitable companion—noise—cannot. Understanding of noise is therefore particularly important for metamaterials. Many performance characteristics can be extracted from models of signal propagation. However, noise models are still at a relatively early stage.

Classically, electromagnetic noise in general media is described using Rytov's theory, originally published in Russian but available in translation[5] and described in standard texts.[6–8] The generation of EM waves—or thermal radiation—from noise is modeled by the addition of further currents or test sources to the Maxwell curl equations. The currents are assumed to be uncorrelated, and their average values are obtained from the imaginary parts of the susceptibility terms using the fluctuation-dissipation (F-D) theorem. This theorem represents a fundamental linkage between loss and noise that was originally derived by Nyquist[9] following experimental measurement of noise in resistors by Johnson[10] and later generalized to other lossy systems.[11–13] The theory has been applied to calculation of the emission from plasmas,[14–17] and more recently to photonic band-gap media.[18–20] For electrical circuits, noise is typically represented using current and voltage sources, whose average values are again obtained from the F-D theorem.[21] In periodic circuits, or circuits containing distributed interconnects, these sources again lead to the propagation of noise waves.[22–27]

Metamaterials are often represented using equivalent circuits.[28–32] Using this approach, noise models may be constructed by adding suitable current and voltage sources, and solving simple circuit equations to find their cumulative effects. However, in the limit, such models should yield the results obtained from the use of effective medium properties in rigorous EM theory. In a series of papers, we have been attempting to demonstrate the required correspondence. Our first paper considered noise in split-ring resonator (SRR) arrays, such as the linear array of coupled resonators in Fig. 1(a).[33] Coupling to EM waves was neglected, leaving the noise trapped in the array and propagating as internal lattice waves, equivalent to the well-known magnetoinductive (MI) waves.[34] Others have also considered noise in magnetoinductive communications systems.[35] Our second considered the additional effect of coupling to a suitably polarized EM wave propagating parallel to the axis of the array, as shown in Fig. 1(b).[36] This model allowed noise to be transferred to the EM wave, and demonstrated the inherent link between effective permeability and noise. Our third considered the additional effect of rod loading, as shown in Fig. 1(c).[37] This model allowed the contributions of the effective permeability and permittivity to the noise to be separately identified. However, to simplify the mathematics, coupling between the resonators was ignored, eliminating the possibility of MI waves. Since then, a new model has been developed that treats the properties of an entire uniform slab, including its noise, as those of a lossy four pole.[38] This approach presents an elegant simplification, especially for calculations involving thick layers, but obscures the internal detail of the noise.

Each of the structures in Fig. 1 is clearly one dimensional. An important question is whether models such as Figs. 1(b)

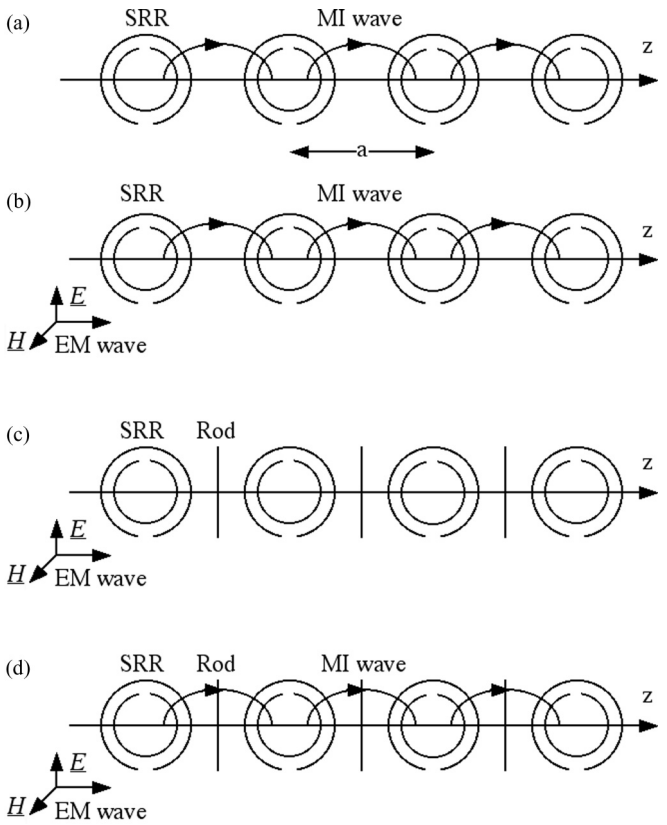

FIG. 1. Models for 1D metamaterials: (a) magnetoinductive waveguide, (b) magnetic metamaterial, and [(c), (d)] negative-index metamaterial, without and with magnetoinductive lattice waves, respectively.

and 1(c) may be used to represent perpendicular incidence of a plane wave on a slab of a three-dimensional lattice, for which the effective permeability and permittivity could have their conventional meaning. In fact, it is simple to show that for waves propagating parallel to a principal axis of a cubic lattice, the only effect of magnetic coupling in the two perpendicular directions is to alter the apparent inductance of the resonant loops. However, for propagation in an arbitrary direction, and more complex unit cells, a full three-dimensional treatment is required. Such a treatment would naturally lead to tensor definitions of the effective medium properties, and careful treatment of the boundaries (which might or might not lie parallel to a principal axis) would be required.

In this paper, we take our detailed model one step further, and combine resonator loading, rod loading, and resonator coupling to allow lattice waves as shown in Fig. 1(d). A further important question is whether the wires should be considered infinite or not. The former may be represented as an inductive loading, while the latter may clearly be resonant. In addition, cut wires may clearly be coupled end to end or side to side. The former case may be modeled using a capacitive loading.[39] The latter has been shown to lead to additional magnetic (and hence negative index) effects[40] and the propagation of additional lattice waves.[41] Since our aim here is to investigate the linkage between signal propagation and noise in a material supporting internal lattice waves, we assume the simplest example, namely, the case when the wires are infinite and uncoupled. The model is introduced in Sec. II. The effective medium properties are derived in Sec. III, example noise performance is calculated in Sec. IV, and conclusions are drawn in Sec. V.

II. EQUIVALENT CIRCUIT MODEL

The system of Fig. 1(d) is modeled as the equivalent circuit shown in Fig. 2(a). The EM wave is represented by a lossless transmission line, with series inductance $L_0 = \mu_0 a$ and shunt capacitance $C_0 = \varepsilon_0 a$ in each section of length a, where $\mu_0 = 4\pi \times 10^{-7}$ H/m and $\varepsilon_0 = 8.85 \times 10^{-12}$ F/m are the permeability and permittivity of free space. SRR loading is modeled as coupling via mutual inductance M_M to a set of lumped-element L-C resonators with inductance L_M (with associated resistance R_M) and capacitance C_M, and nearest-neighbor magnetic coupling between the resonators is described using the mutual inductance M. Rod loading is modeled via the introduction of shunt inductors L_E (with associated resistance R_E).

A finite slab of thickness d of such a medium surrounded by free space can be modeled as a set of $N_{el} = d/a$ sections terminated using loads $Z_0 = \sqrt{\mu_0/\varepsilon_0}$. Propagation through the slab may then be modeled by introducing a signal source at one end, and calculating the transmitted and reflected powers. Here, however, our interest is in thermal noise.

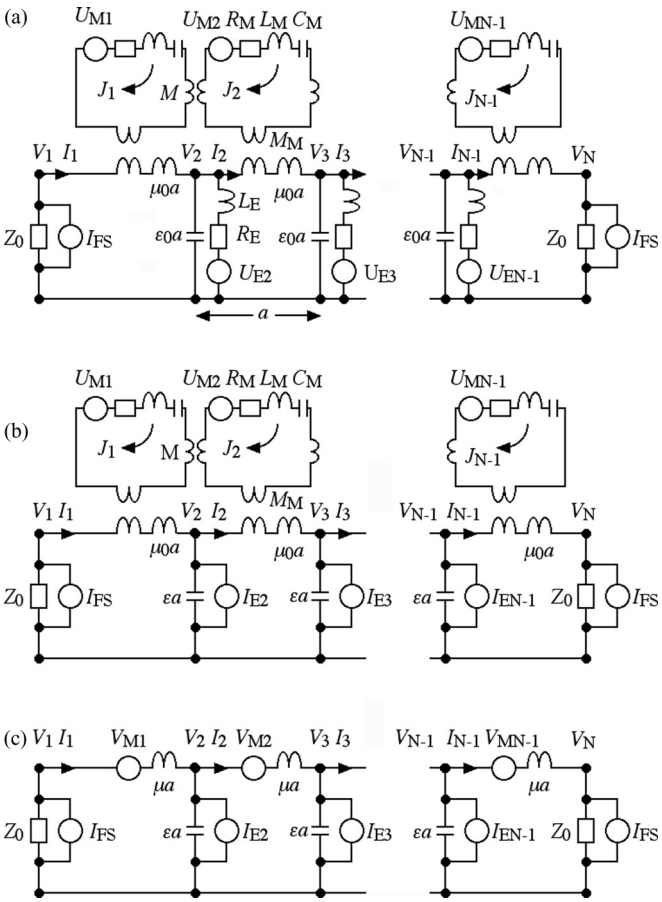

FIG. 2. (a) Transmission line model of a 1D negative-index metamaterial; model after abstraction of (b) the relative permittivity and (c) the relative permeability.

According to Nyquist,[9] any resistive element will have as a companion a series voltage source or a shunt current source that generates noise. In Fig. 2(a), we have represented the sources U_{Mn} and U_{En} associated with the resistors R_M and R_E as voltages. At absolute temperature θ (assumed the same everywhere, so the system is in thermal equilibrium) the RMS voltage of these sources at angular frequency ω in a bandwidth df is defined (at least, at low frequency) as

$$\begin{aligned} U_{Mn}U_{Mn}^* &= 4K\theta R_M df, \\ U_{En}U_{En}^* &= 4K\theta R_E df, \end{aligned} \tag{1}$$

where K is Boltzmann's constant. Here, we have represented the noise associated with the free-space terminations as current sources I_{FS}, whose rms value in a bandwidth df can be written as

$$I_{FS}I_{FS}^* = \frac{4K\theta}{Z_0}df. \tag{2}$$

These sources are needed for the metamaterial slab to remain in thermal equilibrium with its surroundings (a medium of characteristic impedance Z_0, also at temperature θ), and their presence allows a simple method of calculating the noise factor of the slab. In this example, the topology of the shunt branches is simple. Using standard circuit theory, each set of components $C_0 = \varepsilon_0 a$, L_E and R_E can be replaced with an equivalent, frequency-dependent "capacitor" $C = \varepsilon a$. Here $\varepsilon = \varepsilon_0\varepsilon_r$, where $\varepsilon_r = \varepsilon_r' - j\varepsilon_r''$ is the relative permittivity and

$$\varepsilon_r = 1 - \frac{\omega_p^2}{\omega^2 - j\omega\omega_\tau}. \tag{3}$$

Here $\omega_p = 1/\sqrt{L_E C_0}$ and $\omega_\tau = R_E/L_E$ are the equivalent plasma frequency and collision damping frequency of the rods, respectively. Similarly, each voltage source U_{En} can be replaced with a shunt current source I_{En}, such that

$$I_{En}I_{En}^* = 4K\theta\omega\varepsilon_0\varepsilon_r'' a df. \tag{4}$$

With these simple manipulations, the circuit of Fig. 2(a) may be replaced with the entirely equivalent circuit of Fig. 2(b).

In the absence of coupling between the resonators, a similar manipulation can be performed. Each set of components $L_0 = \mu_0 a$, L_M, R_M, and C_M can be replaced with a frequency-dependent "inductor" $L = \mu a$. Here $\mu = \mu_0\mu_r$, where $\mu_r = \mu_r' - j\mu_r''$ is the relative permeability and

$$\mu_r = 1 - \frac{q^2}{1 - \omega_0^2/\omega^2 - j\omega_0/\omega Q_0}. \tag{5}$$

Here $\omega_0 = 1/\sqrt{L_M C_M}$ is the resonant frequency of the resonators, $Q_0 = \omega_0 L_M/R_M$ is their quality factor, and $q^2 = M_M^2/L_0 L_M$ is the filling factor. Similarly, it is simple to show that each voltage source U_{Mn} can be replaced with a series voltage source V_{Mn}, such that

$$V_{Mn}V_{Mn}^* = 4K\theta\omega\mu_0\mu_r'' a df. \tag{6}$$

With these manipulations, the circuit of Fig. 2(b) may be redrawn as Fig. 2(c), as was done in Ref. 37. Two consequences will be immediately apparent. First, components such as resistors, inductors, and capacitors have been replaced with effective medium parameters. Secondly, noise sources whose values depend on resistances have been replaced with sources depending on the imaginary parts of susceptibilities. Thus, a direct correspondence has been achieved with the Rytov theory,[5] and Fig. 2(c) effectively represents a discrete form of the Maxwell curl equations in one dimension. The difficulty, of course, is that this simplification is not immediately possible when there is coupling between the resonators, since the series loading on the EM line is no longer so easily reduced. The remainder of this paper is devoted to determining the implications.

III. EFFECT OF THE LATTICE ON DISPERSION

We start by considering the effect of the lattice on the dispersion of the EM wave. In the presence of coupling between the resonators, Kirchhoff's laws may be used to construct circuit equations relating the voltage V_n and the currents I_n and J_n in the nth section to values in neighboring sections. In the uniform region, we obtain

$$\begin{aligned} V_{n+1} - V_n + j\omega\mu_0 a I_n + j\omega M_M J_n &= 0, \\ I_n - I_{n-1} + j\omega\varepsilon a V_n &= I_{En}, \\ \left(R_M + j\omega L_M + \frac{1}{j\omega C_M}\right)J_n + j\omega M(J_{n-1} + J_{n+1}) & \\ + j\omega M_M I_n &= U_{Mn}. \end{aligned} \tag{7}$$

Similarly, in the terminating elements we obtain

$$\begin{aligned} I_1 + \frac{V_1}{Z_0} &= I_{FS}, \\ -I_{N-1} + \frac{V_N}{Z_0} &= I_{FS}. \end{aligned} \tag{8}$$

Here $N = N_{el} + 1$. In the absence of the noise sources, the terms V_n may be eliminated from Eq. (7) to leave a pair of coupled equations containing only I_n and J_n,

$$\begin{aligned} j\omega\mu_0 a I_n - \frac{I_{n+1} - 2I_n + I_{n-1}}{j\omega\varepsilon a} + j\omega M_M J_n &= 0, \\ \left(R_M + j\omega L_M + \frac{1}{j\omega C_M}\right)J_n + \omega M(J_{n-1} + J_{n+1}) & \\ + j\omega M_M I_n &= 0. \end{aligned} \tag{9}$$

These equations can be written as

$$\begin{aligned} I_n + \frac{\omega_0'^2}{\omega^2\varepsilon_r}(I_{n+1} - 2I_n + I_{n-1}) + \frac{M_M}{L_0}J_n &= 0, \\ \left(1 - \frac{\omega_0^2}{\omega^2} - \frac{j\omega_0}{\omega Q_0}\right)J_n + \frac{\kappa}{2}(J_{n+1} + J_{n-1}) + \frac{M_M}{L_M}I_n &= 0. \end{aligned} \tag{10}$$

Here $\kappa = 2M/L_M$ is the coupling coefficient between the resonant elements (negative in this arrangement) and $\omega_0' = 1/\sqrt{\mu_0\varepsilon_0 a^2}$. Assuming the traveling wave solutions $I_n = I_0\exp(-jnka)$, and $J_n = J_0\exp(-jnka)$, where k is the propagation constant of the combined system, we obtain

$$\begin{aligned} \left[1 + 2\frac{\omega_0'^2}{\omega^2\varepsilon_r}[\cos(ka) - 1]\right]I_0 + \frac{M_M}{L_0}J_0 &= 0, \\ \left[1 - \frac{\omega_0^2}{\omega^2} - \frac{j\omega_0}{\omega Q_0} + \kappa\cos(ka)\right]J_0 + \frac{M_M}{L_0}I_0 &= 0. \end{aligned} \tag{11}$$

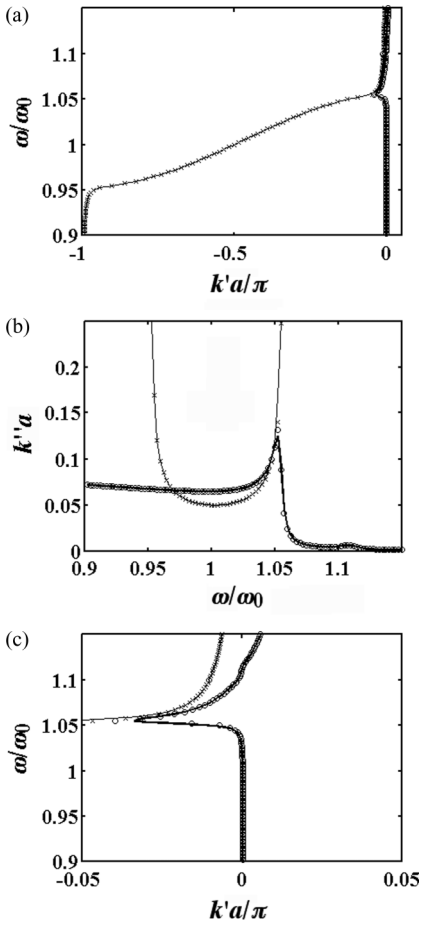

FIG. 3. (a) Dispersion and (b) attenuation characteristics for the model of Fig. 2(b), assuming $\omega_0'/\omega_0 = 10$, $Q_0 = 200$, $\kappa = -0.1$, $q_2 = 0.1$, $\omega_p/\omega_0 = 1.1$, and $\omega_\tau/\omega_0 = 0.01$. Circles and crosses: numerical solution for EM and MI waves; thick and thin lines: analytic solution for EM and MI waves. (c) Expanded view of the dispersion characteristics near the interaction region.

Uncoupling then gives the dispersion equation

$$\left[1 - \frac{\omega_0^2}{\omega^2} - \frac{j\omega_0}{\omega Q_0} + \kappa\,\cos(ka)\right]\left[1 + 2\frac{\omega_0'^2}{\omega^2\varepsilon_r}[\cos(ka) - 1]\right] - q^2 = 0. \quad (12)$$

This equation is a quadratic in $\cos(ka)$, which may be solved for any value of ω, allowing the complex propagation constant $k = k' - jk''$ to be found. Two factors complicate the results. First, there are now two solutions, one corresponding to an EM-like wave, the other to an MI-like wave. Secondly, each value of $\cos(ka)$ has two possible values of $k'a$ within the range $-\pi \leqslant k'a \leqslant \pi$. However, any ambiguity may be removed by selecting the sign of k so that the wave is lossy.

The discrete points in Fig. 3 show frequency variations of (a) the dispersion and (b) the attenuation for the typical parameters $\omega_0'/\omega_0 = 10$, $Q_0 = 200$, $\kappa = -0.1$, $q^2 = 0.1$, $\omega_p/\omega_0 = 1.1$, and $\omega_\tau/\omega_0 = 0.01$, focusing on the important frequency range near ω_0 and ω_p. The EM-like solution (circles) has a small value of $|k'a|$, while the MI-like solution (crosses) extends from $k'a = 0$ down to $k'a = -\pi$. If (as is the case here) the relative permittivity is known analytically, the relative permeability can be extracted from the dispersion relation as

$$\mu_r = \left(\frac{k_{EM}a}{k_0 a}\right)^2 \frac{1}{\varepsilon_r}. \quad (13)$$

Here k_{EM} is the propagation constant of the electromagnetic branch, and $k_0 = \omega\sqrt{\varepsilon_0\mu_0}$ is the corresponding value for an unloaded EM wave. However, rather than extracting μ_r numerically, we note that the main interaction in Fig. 3 occurs when $k'a$ and $k''a$ are both small. In this case, Eq. (12) may be approximated as

$$\left[1 + \kappa - \frac{\omega_0^2}{\omega^2} - \frac{j\omega_0}{\omega Q_0}\right]\left[1 + \frac{\omega_0'^2}{\omega^2\varepsilon_r}k^2a^2\right] - q^2 = 0. \quad (14)$$

Rearranging, we can write the above as

$$1 - \frac{\omega_0'^2}{\omega^2\varepsilon_r\mu_r}k^2a^2 = 0. \quad (15)$$

Here μ_r has the well-known value (see, e.g., Ref. 42)

$$\mu_r = 1 - \frac{q^2}{1 + \kappa - \omega_0^2/\omega^2 - j\omega_0/\omega Q_0}. \quad (16)$$

This result implies that magnetic behavior is still obtained when the resonators are coupled, but the resonance is shifted to a higher frequency $\omega_{0\kappa} = \omega_0/\sqrt{1+\kappa}$. The propagation constant of the EM-like wave can then be written as $k_{EM}a = nk_0a$, where $n = \sqrt{\varepsilon_r\mu_r}$ is the refractive index. This solution is plotted as the thick lines in Figs. 3(a) and 3(b), and also in Fig. 3(c), which shows an expanded view of the dispersion diagram near the region where the two waves interact. For these generally realistic parameters, Eq. (16) is a good approximation. However, its accuracy degrades if q^2 or Q_0 rises significantly, and it becomes extremely inaccurate when losses tend to zero. In this case, anomalous effects start to occur. Particularly, a band emerges near $\omega_{0\kappa}$, for which the imaginary part of μ_r is nonzero, despite the absence of losses.[43]

What of the MI branch of the dispersion diagram? Numerical evaluation shows that, to good approximation, this is still described by the standard MI dispersion equation[34]

$$1 - \frac{\omega_0^2}{\omega^2} - \frac{j\omega_0}{\omega Q_0} + \kappa\,\cos(k_{MI}a) = 0. \quad (17)$$

This solution is plotted as the thin lines in Figs. 3(a)–3(c); it is clearly in excellent agreement with the numerical data for the MI-like branch. Thus, interaction between the electromagnetic wave and the resonator arrays alters the effective medium parameters, without significantly perturbing the properties of any magnetoinductive wave supported by the array. Examination of the eigenvectors (I_0, J_0) of the coupled system reinforces this conclusion; the EM-like eigenvector contains both I_0 and J_0 in varying proportions, while the MI-like eigenvector is always dominated by J_0.

The frequency dependence of the effective medium parameters obtained from Eqs. (3) and (16) is shown in Fig. 4, for (a) the relative permittivity ε_r, (b) the relative permeability μ_r, and (c) the refractive index n. In each case, the real part is shown as a full line and the imaginary part as a

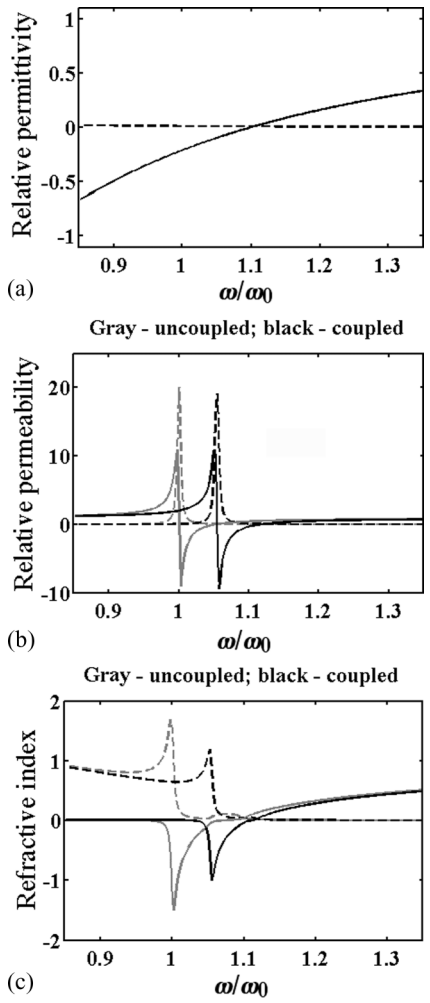

FIG. 4. Frequency dependence of the real (full lines) and imaginary (dashed lines) parts of (a) ε_r and (b) μ_r and n for the model of Fig. 2(b). Assumed parameters are as for Fig. 3, but with $\kappa = 0$ (gray) and $\kappa = -0.1$ (black).

dashed line. The parameter values are generally as before. However, two sets of data are shown for μ_r and n: without coupling between the resonators ($\kappa = 0$, in gray) and with coupling ($\kappa = -0.1$, in black). The results are in agreement with those obtained by many previous authors. The real part of ε_r changes monotonically with frequency, and is clearly negative for $\omega < \omega_p$. The real part of μ_r in contrast exhibits resonant behavior, and can be negative in a region just above the effective resonance. When ε_r and μ_r are both positive, the refractive index is positive. Conversely, when they are both negative, n can be negative. However, magnetic coupling clearly has the effect of reducing the frequency range over which this can occur.

Finally, we note that, given the approximations to the dispersion diagram made so far, the standard expression $Z_{EM} = \sqrt{\mu_0\mu_r/\varepsilon_0\varepsilon_r}$ must also represent an accurate analytic approximation for the characteristic impedance of the EM-like wave. Similarly, the well-known expression $Z_{MI} = j\omega\ M\ \exp(-jk_{MI}a)$ is a useful approximation for the impedance of the MI-like wave.

IV. EFFECT OF THE LATTICE ON NOISE

We now consider the effect of the lattice on the thermal noise. To find the noise, we must solve Eqs. (7) and (8), assuming the presence of a set of incoherent noise sources. To do so, we note that the equations can be written together in matrix form as $\mathbf{MY} = \mathbf{X}$. Here $\mathbf{M}$ is an $M \times M$ matrix containing the admittances and impedances, $\mathbf{Y}$ is an M-element column vector containing the nodal voltages and line currents, and $\mathbf{X}$ is an M-element column vector containing the noise voltages and currents, where $M = 3N_{el} + 1$. The unknowns can clearly be found for any input as $\mathbf{Y} = \mathbf{M}^{-1}\mathbf{X}$. Since the sources are not correlated, the local noise due to the material may be found directly, by evaluating $\mathbf{Y}$ for each source in turn and performing an incoherent addition of the results.

For example, to find the effect at an observation point at element n inside the array, the magnetic and electric sources are applied at locations m in turn and the resulting powers are simply summed. Assuming the currents due to magnetic and electric sources are I_{Mnm} and I_{Enm}, respectively, the local noise power in the EM wave is then $P_{EMn} = P_{EM\_Mn} + P_{EM\_En}$, where

$$P_{EM\_Mn} = \sum_m I_{Mnm} I^*_{Mnm}\,\mathrm{Re}(Z_{EM}),$$
$$P_{EM\_En} = \sum_m I_{Enm} I^*_{Enm}\,\mathrm{Re}(Z_{EM}). \tag{18}$$

These powers may be converted into spectral densities p_{EM_Mn}, p_{EM_En}, and p_{EMn}, such that $p_{EM\_Mn} = P_{EM\_Mn}/df$, and so on. Similarly, the power delivered to (say) the right-hand load—the emitted power—is $P_{EM} = P_{EM\_M} + P_{EM\_E}$, where

$$P_{EM\_M} = \sum_m I_{MNm} I^*_{MNm}\,\mathrm{Re}(Z_0),$$
$$P_{EM\_E} = \sum_m I_{ENm} I^*_{ENm}\,\mathrm{Re}(Z_0). \tag{19}$$

These powers may be again converted into spectral densities p_{EM_M}, p_{EM_E}, and p_{EM} using division by df. The emittance may then be found as the ratio of the emitted power to the maximum available power, namely,

$$E = \frac{p_{EM}}{K\theta}. \tag{20}$$

Similarly, by considering the alteration of the signal-to-noise ratio (SNR) of a signal wave, it is simple to show that the noise factor is (see, e.g., Ref. 37 for details)

$$F = 1 + \frac{E}{T}. \tag{21}$$

Here T is the power transmittance of the slab, which can be found numerically by placing a signal source in the left-hand element and calculating the relative power dissipated in the RH element. The noise factor is often plotted in dB as the noise figure $10\ \log_{10}(F)$.

The frequency dependence of these quantities is shown in Fig. 5, for (a) the EM noise at the center of the array, (b) the emittance, and (c) the noise factor. Once again, the parameters are as before, and results are shown for an array containing $N_{el} = 101$ elements. Two sets of data are

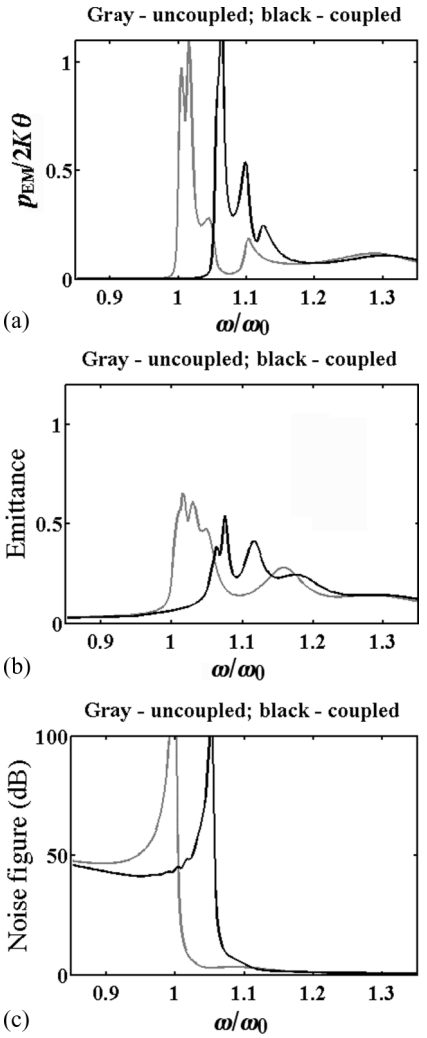

FIG. 5. Frequency dependence of (a) power spectral density of the EM noise at the slab center, (b) emittance, and (c) noise figure for the model of Fig. 2(b). Assumed parameters are as for Fig. 3, but with $N_{el} = 101$, $\kappa = 0$ (gray), and $\kappa = -0.1$ (black).

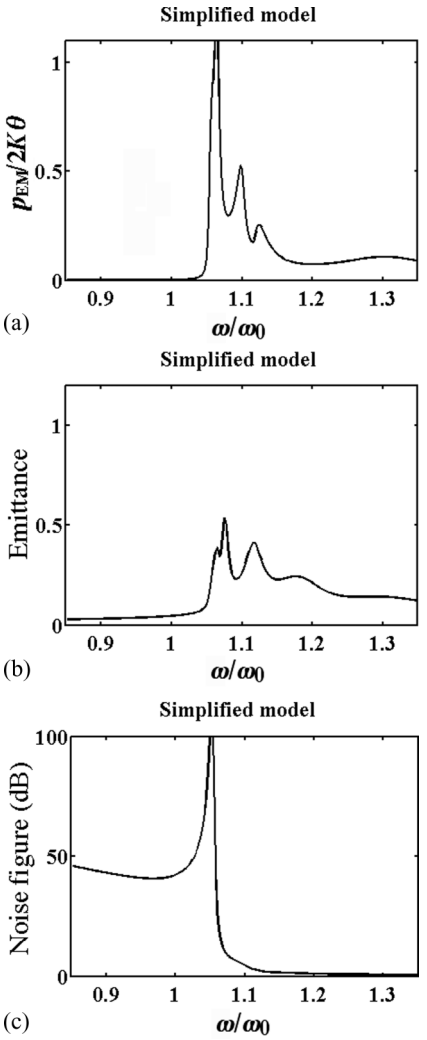

FIG. 6. Frequency dependence of the spectral density of the EM noise at the slab center, (b) emittance, and (c) noise figure for the model of Fig. 2(c). Assumed parameters are as for Fig. 3, but with $N_{el} = 101$ and $\kappa = -0.1$.

again provided: without coupling between the resonators ($\kappa = 0$, in gray) and with coupling ($\kappa = -0.1$, in black). Since the variations are generally similar to results previously presented in Ref. 37, only the main points will be discussed.

In each case, separate examination of the magnetic and electric contributions shows that magnetic noise arising from the lossy resonators dominates in the crucial region where the effective index can be negative. The effect of coupling between the resonators is also to upshift the frequency where the magnetic noise is significant, so that the noise remains inescapably linked to the effective medium properties. The frequency dependence of the power spectral density of the internal noise (p_{EM}) is relatively complicated, but in the limit of a very thick slab, its value tends to $2K\theta$ (corresponding to $K\theta$ per wave direction) in the two propagating bands where losses are low, as was shown in Ref. 37. The frequency dependence of the emittance E is also complicated, but again tends to a limit for very thick slabs. The noise figure clearly rises rapidly as the effective magnetic resonance is approached, and this poor performance represents a key limitation of metamaterials. Particularly, it may prevent large values of negative index (which are only obtained close to the magnetic resonance) being exploited in practical applications unless the Q factor is high.

All the results above were obtained using the model of Fig. 2(b). Interestingly, the same results can be obtained to a very high degree of approximation using the model of Fig. 2(c),[36] simply by using the appropriate frequency variations of Eqs. (3) and (16) for ε_r and μ_r. For example, Figs. 6(a)–6(c) show results corresponding to those of Figs. 5(a)–5(c), obtained from the simplified model for the case when $\kappa = -0.1$; they are for all practical purposes identical. This initially surprising conclusion implies that the details of any internal lattice waves must be completely unimportant in determining the electromagnetic noise, but is entirely consistent with the abstraction of the effective medium parameters and their associated losses into the reduced

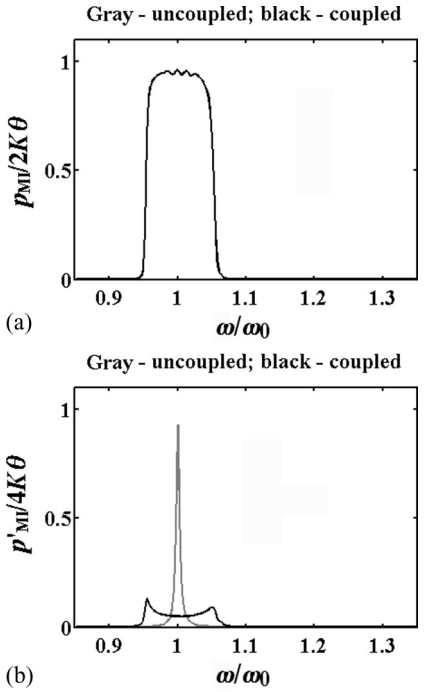

FIG. 7. Frequency dependence of the power spectral density of (a) propagating and (b) dissipated MI noise at the slab center for the model of Fig. 2(b). Assumed parameters are as for Fig. 3, but with $\kappa = 0$ (gray) and $\kappa = -0.1$ (black).

representation of Fig. 2(c). On this basis we may expect that the same results will also be obtained using further abstraction to the simplest possible four-pole representation of Ref. 38.

The lattice waves must, nonetheless, be present. By analogy, the local magnetoinductive noise inside the array may be found as $P_{MIn} = P_{MI\_Mn} + P_{MI\_En}$, where

$$P_{MI\_Mn} = \sum_m J_{Mnm} J^*_{Mnm} \,\mathrm{Re}(Z_{MI}),$$
$$P_{MI\_En} = \sum_m J_{Enm} J^*_{Enm} \,\mathrm{Re}(Z_{MI}). \tag{22}$$

Note that alternative quantities may be defined for magnetoinductive power (for example, as was done in Ref. 33) as $P'_{MIn} = P'_{MI\_Mn} + P'_{MI\_En}$, where

$$P'_{MI\_Mn} = \sum_m J_{Mnm} J^*_{Mnm} R_M,$$
$$P'_{MI\_En} = \sum_m J_{Enm} J^*_{Enm} R_M. \tag{23}$$

Each expression has particular advantages. The quantities in Eq. (22) represent local flow of magnetoinductive power, and may be useful in SNR calculations involving signal propagation in MI waveguides. In contrast, those in Eq. (23) represent local dissipation of magnetoinductive power. However, they are easily measurable with a near-field probe, and as a result the existence of magnetoinductive noise waves may be confirmed experimentally.

Figure 7 shows the frequency dependence of (a) propagating and (b) dissipated magnetoinductive noise at the center of the array. Once again, the parameters are generally as before, and results are computed for an array with $N_{el} = 101$ elements. Two sets of data are again shown: without coupling between the resonators ($\kappa = 0$, in gray) and with coupling ($\kappa = -0.1$, in black). In the absence of coupling, there is clearly no propagating MI noise, and the power spectral density of the dissipated MI noise approximates to that found in a single lossy resonator, with a single peak near $\omega = \omega_0$. When the coupling is present, propagating MI noise exists over the whole of the MI wave band. Once again its power spectral density approximates to $2K\theta$, and because the MI propagation losses are higher, it does so more quickly than the EM wave. The power spectral density of the dissipated noise is also spread over the MI band, but its average value is reduced to maintain the total dissipation (as was previously found in Ref. 33).

Numerically, we have verified that all the other results for the different one-dimensional media previously presented in Refs. 33, 36, and 37 are obtainable as special cases using the new model, confirming that it describes all phenomena present in Fig. 1.

V. CONCLUSIONS

We have demonstrated a one-dimensional equivalent circuit model for thermal noise in a slab of negative-index metamaterial based on rods and split-ring resonators, including the effect of nearest-neighbor magnetic coupling between the resonators. The noise is represented by a set of mutually incoherent voltage sources, whose values are obtained from the fluctuation-dissipation theorem. As is commonly accepted, rod loading provides an effective nonunity value of relative permittivity ε_r. Similarly, SRR loading provides an effective value of relative permeability μ_r, with any magnetic coupling shifting the apparent resonance of the SRRs up in frequency. However as we show here, another effect of coupling is to allow propagation of magnetoinductive noise waves. By comparing two models—one explicitly detailing the magnetoinductive lattice and the other containing only the modified effective medium properties—we show that the power spectral density of the electromagnetic noise inside or outside the medium may be derived entirely from the extracted values of ε_r and μ_r. All related quantities such as the noise factor then follow directly. This simple result is entirely as expected from the fluctuation-dissipation theorem, and we conjecture that the same general result will hold for other media, namely, that their noise performance may be computed entirely from their effective medium properties. However, it ignores the magnetoinductive noise trapped in the resonator array, which is directly accessible for measurement using a near-field probe.

ACKNOWLEDGMENTS

The financial support of the Leverhulme Trust is gratefully acknowledged, as are valuable discussions with Ekaterina Shamonina and Mike Wiltshire.

*r.syms@imperial.ac.uk

[1] J. B. Pendry, A. J. Holden, D. J. Robbins, and W. J. Stewart, IEEE Trans. Microwave Theory Tech. **47**, 2075 (1999).

[2] D. R. Smith, W. J. Padilla, D. C. Vier, S. C. Nemat-Nasser, and S. Schultz, Phys. Rev. Lett. **84**, 4184 (2000).

[3] R. A. Shelby, D. R. Smith, and S. Schultz, Science **292**, 77 (2001).

[4] V. G. Veselago, Sov. Phys. Usp. **10**, 509 (1968) [Usp. Fiz. Nauk **92**, 517 (1967)].

[5] S. M. Rytov, *Theory of Electrical Fluctuations and Thermal Radiation* (Academy of Sciences, Moscow, 1953).

[6] L. D. Landau and E. M. Lifschitz, *Electrodynamics of Continuous Media* (Pergamon Press, Oxford, 1984).

[7] S. Kogan, *Electronic Noise and Fluctuations in Solids* (Cambridge University Press, Cambridge, 1996).

[8] H. L. Pesceli, *Fluctuations in Physical Systems* (Cambridge University Press, Cambridge, 2000).

[9] H. Nyquist, Phys. Rev. **32**, 110 (1928).

[10] J. B. Johnson, Phys. Rev. **32**, 97 (1928).

[11] H. B. Callen and T. A. Welton, Phys. Rev. **83**, 34 (1951).

[12] J. Weber, Phys. Rev. **101**, 1620 (1956).

[13] R. Kubo, Rep. Prog. Phys. **29**, 255 (1966).

[14] J. M. Boyd, Phys. Fluids **7**, 59 (1964).

[15] R. P. Mercier, Proc. Phys. Soc. **83**, 819 (1964).

[16] T. Birmingham, J. Dawson, and C. Oberman, Phys. Fluids **8**, 297 (1965).

[17] G. Bekefi, *Radiation Processes in Pplasmas* (Wiley, New York, 1996).

[18] C. M. Cornelius and J. P. Dowling, Phys. Rev. A **59**, 4736 (1999).

[19] C. Luo, A. Narayanaswamy, G. Chen, and J. D. Joannopoulos, Phys. Rev. Lett. **93**, 213905 (2004).

[20] D. L. C. Chan, M. Soljacic, and J. D. Joannopoulos, Phys. Rev. E **74**, 036615 (2006).

[21] H. Rothe and W. Dahlke, Proc. IRE **44**, 811 (1956).

[22] P. Penfield, IRE Trans. Circuit Theory **CT-9**, 83 (1962).

[23] H. Bosma, Ph.D. thesis, Technische Hogeschool Eindhoven, 1967.

[24] R. P. Meys, IEEE Trans. Microwave Theory Tech. **26**, 34 (1976).

[25] R. P. Hecken, IEEE Trans. Microwave Theory Tech. **MTT-29**, 997 (1981).

[26] N. G. Kanaglekar, R. E. McIntosh, and W. E. Bryant, IEEE Trans. Microwave Theory Tech. **MTT-35**, 112 (1987).

[27] S. Withington, Microwave J. **32**, 169 (1989).

[28] M. Rahman and M. A. Stuchly, Microwave Opt. Technol. Lett. **30**, 15 (2001).

[29] G. V. Eleftheriades, A. K. Iyer, and P. C. Kremer, IEEE Trans. Microwave Theory Tech. **50**, 2702 (2002).

[30] G. V. Eleftheriades, O. Siddiqui, and A. K. Iyer, IEEE Microw. Wirel. Compon. Lett. **13**, 31 (2003).

[31] J. D. Baena, J. Bonache, F. Martin, R. Marques, F. Falcone, T. Lopetegi, M. A. G. Laso, J. Garcia-Garcia, M. F. Portillo, and M. Sorolla, IEEE Trans. Microwave Theory Tech. **53**, 1451 (2005).

[32] R. R. A. Syms, E. Shamonina, V. Kalinin, and L. Solymar, J. Appl. Phys. **97**, 064909 (2005).

[33] R. R. A. Syms and L. Solymar, J. Appl. Phys. **109**, 124909 (2011).

[34] E. Shamonina, V. A. Kalinin, K. H. Ringhofer, and L. Solymar, Electron. Lett. **38**, 371 (2002).

[35] C. J. Stevens, C. W. T. Chan, K. Stamatis, and D. J. Edwards, IEEE Trans. Microwave Theory Tech. **58**, 1248 (2010).

[36] R. R. A. Syms, O. Sydoruk, and L. Solymar, Phys. Rev. B **84**, 235150 (2011).

[37] R. R. A. Syms, O. Sydoruk, and L. Solymar, IEEE Trans. Microwave Theory Tech. **61**, 14 (2012).

[38] S. I. Maslovski, C. R. Simovski, S. A. Tretyakov, "Equivalent circuit theory of radiative heat transfer on micro- and nano-scale", Proc. Int. Workshop on Micro-Thermal Radiation, NanoRad'2012, Matsushima Bay Area, Miyagi, Japan, May 23-25, pp. 50–52 (2012) (unpublished).

[39] P. A. Belov, C. R. Simovski, and S. A. Tretyakov, Phys. Rev. E **66**, 036610 (2002).

[40] J. Zhou, L. Zhang, G. Tuttle, T. Koschny, and C. M. Soukoulis, Phys. Rev. B **73**, 041101(R) (2006).

[41] J. Shefer, IEEE Trans. Microwave Theory Tech. **11**, 55 (1963).

[42] M. Gorkunov, M. Lapine, E. Shamonina, and K. H. Ringhofer, Eur. Phys. J. B **28**, 263 (2002).

[43] R. R. A. Syms and L. Solymar, Appl. Phys. Lett. **100**, 124103 (2012).